Perpendicular lamellar-in-lamellar and other planar morphologies in A-b-(B-b-A)(2)-b-C and (B-b-A)(2)-b-C ternary multiblock copolymer melts

Markov, V.; Kriksin, Y.; Erukhimovich, I.; ten Brinke, G.

Published in:
Journal of Chemical Physics

DOI:
10.1063/1.4818872

Perpendicular lamellar-in-lamellar and other planar morphologies in A-b-(B-b-A)2-b-C and (B-b-A)2-b-C ternary multiblock copolymer melts

V. Markov, Y. Kriksin, I. Erukhimovich, and G. ten Brinke

Citation: J. Chem. Phys. **139**, 084906 (2013); doi: 10.1063/1.4818872
View online: http://dx.doi.org/10.1063/1.4818872
View Table of Contents: http://jcp.aip.org/resource/1/JCPSA6/v139/i8
Published by the AIP Publishing LLC.

Perpendicular lamellar-*in*-lamellar and other planar morphologies in A-*b*-(B-*b*-A)$_2$-*b*-C and (B-*b*-A)$_2$-*b*-C ternary multiblock copolymer melts

V. Markov,[1] Y. Kriksin,[2] I. Erukhimovich,[3,4] and G. ten Brinke[1]
[1]*Department of Polymer Chemistry and Zernike Institute for Advanced Materials, University of Groningen, Nijenborgh 4, 9747 AG Groningen, The Netherlands*
[2]*Keldysh Institute of Applied Mathematics, RAS, Moscow 125047, Russia*
[3]*Moscow State University, Moscow 119991, Russia*
[4]*Institute of Organoelement Compounds, RAS, Moscow 119991, Russia*

(Received 6 June 2013; accepted 6 August 2013; published online 29 August 2013)

Ordered planar morphologies in A-*b*-(B-*b*-A)$_2$-*b*-C and (B-*b*-A)$_2$-*b*-C terpolymer melts are studied within the framework of the self-consistent field theory for volume fractions of components A, B, and C in the ratio 1:1:2 and the Flory-Huggins interaction parameters satisfying $\chi_{AB} = 2\chi_{AC}$. The stable phases turn out to be the disordered, hexagonal, parallel lamellar-*in*-lamellar $L_\parallel$ (including the simple lamellar) as well as non-shifted and shifted ($L_\perp$ and $SL_\perp$) perpendicular lamellar-*in*-lamellar morphologies. Depending on the value of the ratio $r = \Theta_{AB}/\Theta_{BC}$, where Θ is a characteristic temperature of the units involved, different sequences of phase transitions are shown to occur. The hexagonal phase is characteristic for $r \cong 1$. The $L_\perp$ and $SL_\perp$ morphologies occur at weak and intermediate segregations whereas the $L_\parallel$ morphology appears for stronger degrees of segregation. For (B-*b*-A)$_2$-*b*-C a reduction in r favors the shifted $SL_\perp$ phase over the non-shifted $L_\perp$ one, whereas for A-*b*-(B-*b*-A)$_2$-*b*-C we find re-entrant phase transitions $SL_\perp - L_\perp$. The physics determining the particular phase behavior is discussed. © *2013 AIP Publishing LLC*. [http://dx.doi.org/10.1063/1.4818872]

I. INTRODUCTION

One of the most interesting features of multiblock copolymer systems is their ability to self-assemble in periodical hierarchical structures involving different length scales. This phenomenon became an attractive area of research both experimentally[1–12] and theoretically,[13–29] during the last decades. First, the two-length-scale structures, which might be called lamellar-*in*-lamellar structures (see Fig. 1), were experimentally studied in detail for comb-shaped supramolecules consisting of polystyrene-*block*-poly(4-vinylpyridine) (PS-*b*-P4VP) diblock copolymers and pentadecylphenol (PDP) side chains attached by hydrogen bonding to the P4VP blocks.[1–3] Next, linear multiblock copolymers P2VP-*b*-(PI-*b*-PS)$_4$-*b*-PI-*b*-P2VP,[4] PS-*b*-(PI-*b*-PS)$_4$-*b*-PI-*b*-PS,[5] and PS-*b*-(P*p*HS-*b*-PS)-*b*-P*p*HS[6] were experimentally studied (P2VP, PI, PS, and P*p*HS denote poly(2-vinylpyridine), polyisoprene, polystyrene, and poly(*p*-hydroxystyrene), respectively). For the symmetric compositions selected these copolymers form so-called *parallel* lamellar-*in*-lamellar structures[4–6] (see Fig. 1).

The *perpendicular* lamellar-*in*-lamellar structure was discovered by Fleury and Bates[7,8] in C-E-C-E-C-P terpolymers, consisting of cyclohexylethylene (C), ethylene (E), and propylene (P) blocks in ratio of 1:1:2 (see Fig. 1). Several other examples of hierarchical structures can be found in Refs. 9–13.

The morphologies occurring in multiblock copolymers with various architectures and interaction parameters were studied theoretically both within the weak[14–17] and strong segregation approach (SSA)[18–21] as well as within the framework of the self-consistent field theory (SCFT).[22–29] In particular, the transitions between the parallel lamellar-*in*-lamellar structures $L_{||}(n)$ with different numbers n of thin layers per large period were studied via the SSA[18–20] and SCFT.[23,25–27,29] The transition between the perpendicular lamellar-*in*-lamellar structure ($L_\perp$) and the parallel ones $L_{||}(n)$ was studied via the SSA,[21] the $L_\perp$ phase being found to become stable for C-E-C-E-C-P-like systems when the interaction parameters satisfy the condition $0 < \chi_{EP} < 0.22\chi_{CP}$). Lines dividing 2D sections of the interaction parameter space (χ_{AB}, χ_{AC}, χ_{BC}) corresponding to the $L_\perp$ and $L_{||}(n)$ stability were obtained via SCFT.[28,29] However, the full phase diagram including not only $L_\perp$ and $L_{||}(n)$ but also hexagonal (HEX) and disordered (DIS) phases has not been built yet. Besides, as explained below, the 2D sections of the full phase diagram chosen in Refs. 28 and 29 are not really physical. Hence, our understanding of the self-assembling in multiblock A-*b*-(B-*b*-A)$_2$-*b*-C (Fig. 2, top) and (B-*b*-A)$_2$-*b*-C (Fig. 2, bottom) terpolymer melts is far from complete and it is the purpose of the present paper to address this.

But the paper is not restricted to this, in addition we will demonstrate that the *perpendicular* lamellar-*in*-lamellar structure occurs in two different varieties called *shifted* and *non-shifted* and evaluate their relative stability. The further presentation is as follows. In Sec. II we describe briefly the model and the basics of the SCFT numerical procedure employed. The phase diagrams are presented and discussed in Sec. III. A brief final summary of our results is given in Sec. IV.

II. MODEL AND THE SCFT TECHNIQUE

Before to remind the reader the basics of the SCFT and pseudo-spectral method we use to solve the SCFT equations

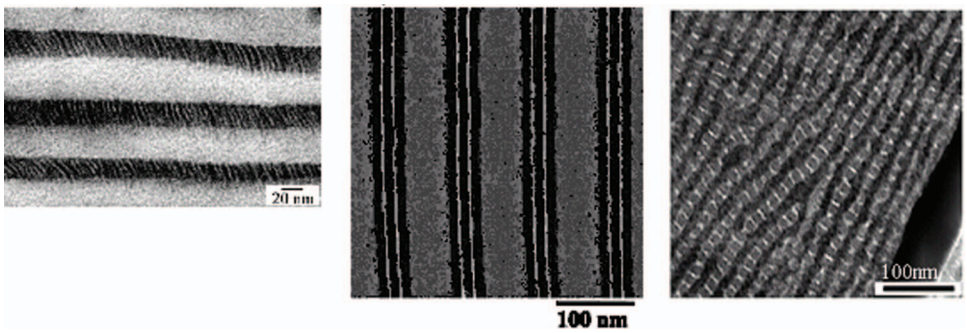

FIG. 1. From left to right: TEM micrographs of the *perpendicular* lamellar-*in*-lamellar structure of PS-*b*-P4VP(PDP) (Reprinted with permission from J. Ruokolainen, R. Mäkinen, M. Torkkeli, T. Mäkelä, R. Serimaa, G. ten Brinke, and O. Ikkala, Science **280**, 557 (1998). Copyright 1998 The American Association for the Advancement of Science), of the *parallel* lamellar-*in*-lamellar structure of P2VP-*b*-(PI-*b*-PS)$_4$-*b*-PI-*b*-P2VP (Reprinted with permission from J. Masuda, A. Takano, J. Suzuki, Y. Nagata, A. Noro, K. Hayashida, and Y. Matsushita, Macromolecules **40**, 4023 (2007). Copyright 2007 American Chemical Society.) and of the *perpendicular* lamellar-*in*-lamellar structure of C-E-C-E-C-P. (Reprinted with permission from G. Fleury and F. S. Bates, Macromolecules **42**, 1691 (2009). Copyright 2009 American Chemical Society.)

we find it useful first to describe the general ways to solve them. The strategies to solve the SCFT equations are the spectral method[30] and the real-space method.[31–35] The first strategy is based on the representation of the spatially varying density fields in a Fourier-type basis, using a large number of harmonic terms.[36] The second computational formalism employs an appropriate relaxation iterative procedure in order to reach a local minimum of the free energy functional, adjusting simultaneously the chemical potential fields and the conjugate monomer densities at every iteration step.

Both schemes have advantages and disadvantages. A disadvantage of the fully spectral schemes is that the computational effort per single iteration scales very poorly as M^3, where M is the number of basis functions. Besides, it requires the symmetry of the microstructures formed to be specified in advance so that a proper set of harmonic terms can be utilized. The real-space methods do not require the system symmetry in advance but are rather time consuming in three dimensions even on supercomputers. Recent progress in this field has been achieved by using the so-called pseudo-spectral technique.[37–40] In the context of polymer physics, this technique was first applied by Rasmussen and Kalosakas[38] in order to solve the modified diffusion equation that describes the propagation of monomer densities. Subsequently, Ceniceros and Fredrickson[39] further extended the approach. In particular, they introduced a robust class of semi-implicit numerical methods that employ supplementary information about the nonlocal density operators. As a result, the total computational cost has been reduced by an order of magnitude. Another way to speed up convergence of the SCFT equations for polymeric systems, we employ here, is to use the iterative scheme by Ng,[41] linearizing the solution around stationary points. A similar procedure was used by Thompson *et al.*[42] Recently Stasiak and Matsen have carried out a comparative study of the various numerical algorithms to implement the SCFT calculations.[43]

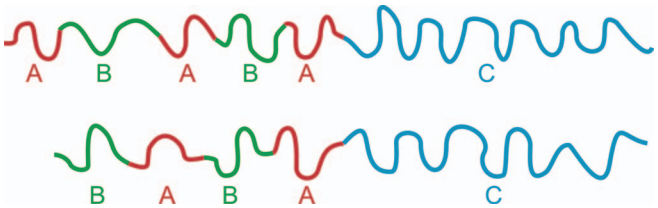

FIG. 2. Ternary multiblock copolymers studied: (a) A-*b*-(B-*b*-A)$_2$-*b*-C; (b) (B-*b*-A)$_2$-*b*-C.

Let us consider an incompressible melt of the linear ternary ABC triblock copolymer chains consisting of the end blocks A and C and the middle block C. The free energy functional for the system under consideration reads:

$$\begin{aligned} F/nk_BT = V^{-1}\int d^3\mathbf{r}[&N\chi_{AB}\lambda_A(\mathbf{r})\lambda_B(\mathbf{r}) + N\chi_{BC}\lambda_B(\mathbf{r})\lambda_C(\mathbf{r}) \\ &+ N\chi_{AC}\lambda_A(\mathbf{r})\lambda_C(\mathbf{r}) - w_A(\mathbf{r})\lambda_A(\mathbf{r}) - w_B(\mathbf{r})\lambda_B(\mathbf{r}) \\ &- w_C(\mathbf{r})\lambda_C(\mathbf{r}) + \xi(\mathbf{r})(\lambda_A(\mathbf{r}) + \lambda_B(\mathbf{r}) + \lambda_C(\mathbf{r}))] \\ &- \ln Q(\{w_\alpha(\mathbf{r})\}), \end{aligned} \tag{1}$$

where the Flory-Huggins parameters $\chi_{\alpha\beta}$ describe the interaction between the monomers of the sorts α and β, V is the volume of the system, N is the degree of polymerization, n is the total number of chains, k_B is Boltzmann constant, and T is the absolute (Kelvin) temperature. Further we set $k_B = 1$, in other words, we measure the temperature in energetic units. $\lambda_\alpha(\mathbf{r})$ is the deviation of the local volume fraction $\varphi_\alpha(\mathbf{r})$ of the αth component from its average (over the volume V) value f_α:

$$\lambda_\alpha(\mathbf{r}) = \varphi_\alpha(\mathbf{r}) - f_\alpha. \tag{2}$$

The quantity $Q(\{w_\alpha(\mathbf{r})\})$ is the partition function of a single ideal chain subject to the external fields $w_\alpha(\mathbf{r})$ acting on the component α,

$$Q(\{w_\alpha(\mathbf{r})\}) = V^{-1}\int d^3\mathbf{r}q(\mathbf{r}, 1), \tag{3}$$

where the density distribution $q(\mathbf{r}, s)$ satisfies the modified diffusion equation,

$$\partial q(\mathbf{r}, s)/\partial s = \nabla^2 q(\mathbf{r}, s) - \psi(\mathbf{r}, s)q(\mathbf{r}, s), \quad q(\mathbf{r}, s) = 1, \tag{4}$$

in which the variable $s \in [0, 1]$ labels the monomer relative distance from an end of the chain, therewith the field $\psi(\mathbf{r}, s) = w_\alpha(\mathbf{r})$ in case the monomer located at a distance s belongs to the sort α. Finally, $\xi(\mathbf{r})$ is the Lagrange multiplier corresponding to the incompressibility condition,

$$\lambda_A(\mathbf{r}) + \lambda_B(\mathbf{r}) + \lambda_C(\mathbf{r}) = 0. \tag{5}$$

The periodic boundary conditions are stipulated on the computation cell boundaries.

Hereafter the products $N\chi_{\alpha\beta}$ in Eq. (1) are replaced by $\tilde{\chi}_{\alpha\beta}$ to simplify the notations. Varying the free energy functional (1) both over the fields $w_\alpha(\mathbf{r})$ and volume fractions $\varphi_\alpha(\mathbf{r})$, one gets the full set of the self-consistent field equations:

$$w_A(\mathbf{r}) = \tilde{\chi}_{AB}\lambda_B(\mathbf{r}) + \tilde{\chi}_{AC}\lambda_C(\mathbf{r}) + \xi(\mathbf{r}), \tag{6}$$

$$w_B(\mathbf{r}) = \tilde{\chi}_{AB}\lambda_A(\mathbf{r}) + \tilde{\chi}_{BC}\lambda_C(\mathbf{r}) + \xi(\mathbf{r}), \tag{7}$$

$$w_C(\mathbf{r}) = \tilde{\chi}_{AC}\lambda_A(\mathbf{r}) + \tilde{\chi}_{BC}\lambda_B(\mathbf{r}) + \xi(\mathbf{r}), \tag{8}$$

supplemented with the incompressibility condition (5).

The local volume fractions $\varphi_A(\mathbf{r})$, $\varphi_B(\mathbf{r})$, and $\varphi_C(\mathbf{r})$ are determined by the equations,

$$\varphi_A(\mathbf{r}) = \frac{1}{Q[w_A, w_B, w_C]}\int_0^1 ds\sigma_A(s)q(\mathbf{r}, s)\tilde{q}(\mathbf{r}, 1-s), \tag{9}$$

$$\varphi_B(\mathbf{r}) = \frac{1}{Q[w_A, w_B, w_C]}\int_0^1 ds\sigma_B(s)q(\mathbf{r}, s)\tilde{q}(\mathbf{r}, 1-s), \tag{10}$$

$$\varphi_C(\mathbf{r}) = \frac{1}{Q[w_A, w_B, w_C]}\int_0^1 ds\sigma_C(s)q(\mathbf{r}, s)\tilde{q}(\mathbf{r}, 1-s), \tag{11}$$

where $\sigma_\alpha(s) = 1$ if the monomer located at a distance s belongs to the sort α and $\sigma_\alpha(s) = 0$ otherwise.

The distribution function $\tilde{q}(\mathbf{r}, s)$ satisfies the modified diffusion equation

$$\partial\tilde{q}(\mathbf{r}, s)/\partial s = \nabla^2\tilde{q}(\mathbf{r}, s) - \psi(\mathbf{r}, 1-s)\tilde{q}(\mathbf{r}, s), \quad \tilde{q}(\mathbf{r}, 0) = 1, \tag{12}$$

with the same boundary conditions as in case of Eq. (4).

The auxiliary field $\xi(\mathbf{r})$, which grants that the incompressibility condition (5) is fulfilled, can be expressed in terms of the fields $\{w_\alpha(\mathbf{r})\}$, and the local volume fractions $\{\varphi_\alpha(\mathbf{r})\}$ and, thus, eliminated:

$$\xi = \frac{1}{3}(w_A + w_B + w_C + \tilde{\chi}_{AB}\lambda_C + \tilde{\chi}_{BC}\lambda_A + \tilde{\chi}_{AC}\lambda_B), \tag{13}$$

following from Eqs. (5)–(8), where $\lambda_\alpha(\mathbf{r}) = \varphi_\alpha(\mathbf{r}) - f_\alpha$ are evaluated using the integral operators (9)–(11). The use of Eq. (13) gives the following converging iterative method.

The set of equations (5)–(12) can be represented as a nonlinear operator equation,

$$x = A[x], \tag{14}$$

with respect to an unknown vector-function,

$$x = (w_A(\mathbf{r}), w_B(\mathbf{r}), w_C(\mathbf{r})). \tag{15}$$

Here the operator A is defined as follows:

$$A[x] = \begin{pmatrix} \tilde{\chi}_{AB}\lambda_B(\mathbf{r}) + \tilde{\chi}_{AC}\lambda_C(\mathbf{r}) + \xi(\mathbf{r}) \\ \tilde{\chi}_{AB}\lambda_A(\mathbf{r}) + \tilde{\chi}_{BC}\lambda_C(\mathbf{r}) + \xi(\mathbf{r}) \\ \tilde{\chi}_{AC}\lambda_A(\mathbf{r}) + \tilde{\chi}_{BC}\lambda_B(\mathbf{r}) + \xi(\mathbf{r}) \end{pmatrix}. \tag{16}$$

The functions $\lambda_\alpha(\mathbf{r})$ are expressed in terms of vector x (i.e., of the fields $w_A(\mathbf{r})$, $w_B(\mathbf{r})$, and $w_C(\mathbf{r})$) via the integral operators (9)–(11). The auxiliary field $\xi(\mathbf{r})$ is given via equality (13). The operator equation (14) can be solved using the Picard iteration procedure,

$$x_{n+1} = x_n + \tau(A[x_n] - x_n), \quad n = 0, 1, 2, \ldots, \tag{17}$$

with a positive parameter τ.

To speed up the iteration procedure convergence, after a certain number of Picard iterations (17) one should switch to the iteration method by Ng, which is characterized by a faster convergence. The details of the Ng method are described in Refs. 24 and 41.

The parameters of the calculations were chosen as follows: the contour step size was taken to be equal to $\Delta s = 0.01$, smaller values were also tested but they did not change the free energy value. The simulation was done in two dimensions with periodic boundary conditions because all experimentally observed structures are 2D. The free energy was optimized with respect to the size and shape of the simulation box.[44–46]

The spatial resolution was equal to $\Delta x = 0.03R_g$, $\Delta y = 0.015R_g$. The numerical simulations proceeded until the relative free energy changes for iteration are smaller than 10^{-5} k_BT per chain and the incompressibility condition became satisfied with an accuracy up to 10^{-4}.

III. RESULTS AND DISCUSSION

The final goal of theoretical investigations in the field of block copolymer ordering (microphase separation) is to find the relationship between the architecture (including the composition) and interaction parameters (including the temperature), on the one hand, and the type of morphology formed. Unfortunately, the plurality of the morphologies which can exist (at least, as metastable ones) given the parameters of the system under consideration makes it difficult to achieve this goal effectively. So, any actual calculation starts from a more or less (but never fully) validated pre-assignment, which morphologies are expected to be the most natural candidates for becoming the stable phase. As is seen from the TEM micrographs presented in Fig. 1, in our case it is natural to restrict ourselves to the 2D (planar) morphologies only.

More precisely, in this paper we compare the relative stability of the disordered (DIS), conventional hexagonal (HEX), and simple lamellar morphologies (LAM or $L_{||}(1)$), parallel lamellar-*in*-lamellar morphology $L_{||}(n)$ and two types of perpendicular lamellar-*in*-lamellar morphologies: non-shifted designated as $L_\perp$ and shifted designated as $SL_\perp$. We describe these morphologies in more detail below. We calculated the phase diagram for (B-*b*-A)$_2$-*b*-C and A-*b*-(B-*b*-A)$_2$-*b*-C multiblock copolymers using the SCFT numerical procedure outlined in Sec. II. In other words, we explore the space of three reduced χ-parameters $\tilde{\chi}_{AB} = \chi_{AB}N$, $\tilde{\chi}_{AC} = \chi_{AC}N$ and $\tilde{\chi}_{BC} = \chi_{BC}N$ (N being the total length of the multiblock copolymer) and divide it into the regions where a particular phase is stable (which means that the phase has the minimal free energy per chain as compared with the competing morphologies). Since it is difficult to visualize the phase

diagram in the 3D space of these independent reduced χ-parameters, some authors[26–29] fix a value of one of these parameters (usually, that of $\tilde{\chi}_{AC}$) and build the phase diagram in 2D section $(\tilde{\chi}_{AB}, \tilde{\chi}_{BC})|_{\tilde{\chi}_{AC}=const}$. Unfortunately, such a choice is not really physical. Indeed, since the temperature dependence of the χ-parameters is typically the same: $\chi_{\alpha\beta} \sim \Theta_{\alpha\beta}/(2T)$, where T and $\Theta_{\alpha\beta}$ are the actual temperature and a characteristic temperature describing incompatibility of the αth and βth components. (For an incompressible solution of homopolymer chains formed of α-units in the solvent comprised of β-particles, the characteristic temperature $\Theta_{\alpha\beta}$ is precisely the Flory Θ-temperature.) Thus, one cannot independently vary $(\tilde{\chi}_{AB}, \tilde{\chi}_{BC})$ and fix simultaneously $\tilde{\chi}_{AC}$. So, unlike Refs. 26–29, we build the phase diagram in the plane $(\tilde{\chi}_{AB}, \tilde{\chi}_{BC})$ under assumptions that the ratio $r_A = \chi_{AB}/\chi_{AC} = \Theta_{AB}/\Theta_{AC}$ is fixed. Given the chemical structure of the monomers A, B, and C, the ratio $r_B = \chi_{AB}/\chi_{BC} = \Theta_{AB}/\Theta_{BC}$ is also fixed. In other words, the temperature evolution of the morphologies replacing each other is determined by motion along the ray drown from the origin $(\chi_{AB} = 0, \chi_{BC} = 0)$, which corresponds to the infinitely large temperature, at the angle $\alpha = \arctan(\chi_{AB}/\chi_{BC})$ to the abscissa-axis $\tilde{\chi}_{BC}$.

The morphologies arising for the system as the temperature decreases change in the order corresponding to crossing the different regions of the phase diagram by this ray. For the sake of simplicity we chose in this paper $\tilde{\chi}_{AB} = 2\tilde{\chi}_{AC}$, which is not far away from the experimental value $\tilde{\chi}_{AB} = 1.6\,\tilde{\chi}_{AC}$ valid for the Fleury and Bates experiments (See Refs. 7, 8, and references therein). Besides, in accordance with the latter, we assume the component compositions to be $\varphi_C = 0.5$, $\varphi_A = \varphi_B = 0.25$.

The corresponding phase diagrams are presented in Figs. 3 and 4.

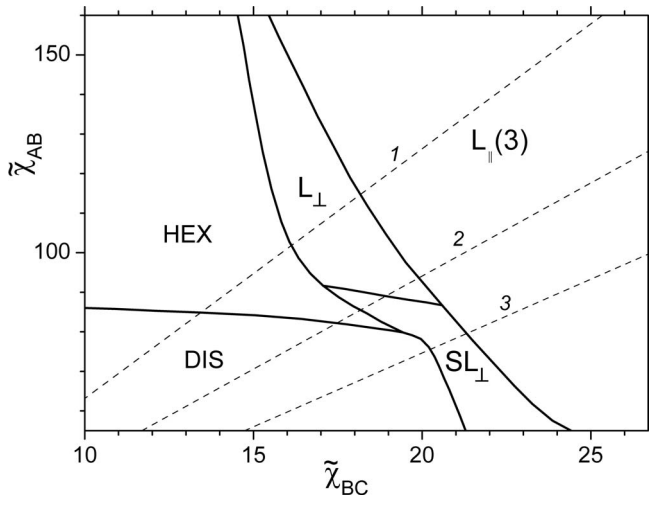

FIG. 3. Phase diagram of (B-*b*-A)$_2$-*b*-C block copolymers in the plane $(\tilde{\chi}_{AB} = 2\tilde{\chi}_{AC}, \tilde{\chi}_{BC})$. The regions where the disordered, hexagonal, parallel, perpendicular, and shifted perpendicular morphologies are stable are denoted as DIS, HEX, $L_{||}$, $L_\perp$ and $SL_\perp$, respectively. The number in between brackets, i.e., $L_{||}(3)$, denotes the total number of "internal" A + B layers. The dashed lines correspond to different types of temperature evolution corresponding to a different choice of A, B, and C monomers. The labels *1, 2, 3* are used in the discussion in the text.

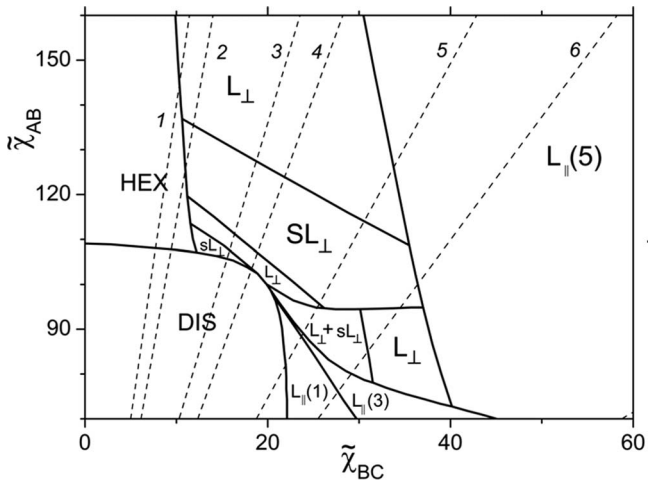

FIG. 4. The phase diagram of A-*b*-(B-*b*-A)$_2$-*b*-C block copolymers in the plane $(\tilde{\chi}_{AB} = 2\tilde{\chi}_{AC}, \tilde{\chi}_{BC})$. The region labeled as $L_\perp + SL_\perp$ is that of coexistence of the phases $L_\perp$ and $SL_\perp$. Other designations are the same as in Fig. 3.

Before we start the discussion about these phase diagrams we first describe the different morphologies found to be stable in more detail.

A. Parallel lamellar-*in*-lamellar morphology $L_{||}(n)$

The morphology $L_{||}(n)$ is characterized by a parallel layered structure, where each layer between successive C-layers contains a total of n A- and B-layers. The number n of "internal" layers is indicated by the number in brackets, i.e., $L_{||}(3)$ denotes 3 internal layers (A-B-A). In particular, $L_{||}(1)$ is just the conventional lamellar morphology similar to that observed in AB diblock copolymers. The actual value of n is determined by the multiblock copolymer architecture and the values of the interaction parameters.

To describe the morphologies $L_{||}(n)$ in more detail we will consider the composition profiles for various points of the phase diagrams. Figure 5 shows the composition profile of

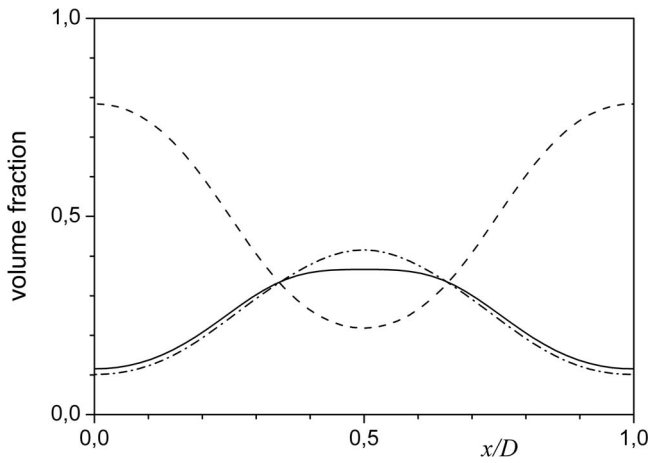

FIG. 5. Volume fraction profiles of A-*b*-(B-*b*-A)$_2$-*b*-C indicating a simple lamellar structure for $\tilde{\chi}_{AB} = 2\tilde{\chi}_{AC} = 80$ and $\tilde{\chi}_{BC} = 24$. The solid, dotted–dashed, and dashed lines correspond to the profiles of the A, B, and C components, respectively.

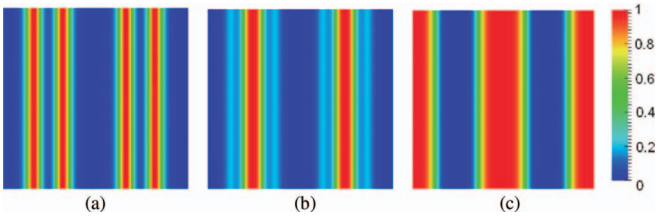

FIG. 6. Volume fraction maps for the parallel lamellar-*in*-lamellar $L_{||}(3)$ structure of A-*b*-(B-*b*-A)$_2$-*b*-C with two A-type internal layers at $\tilde{\chi}_{AB} = 2\tilde{\chi}_{AC} = 100$ and $\tilde{\chi}_{BC} = 40$. (a) A blocks; (b) B blocks; (c) C blocks.

A-*b*-(B-*b*-A)$_2$-*b*-C for $\tilde{\chi}_{AB} = 2\tilde{\chi}_{AC} = 80$ and $\tilde{\chi}_{BC} = 24$. Even though the absolute value of the AB interaction parameter is the biggest, it is insufficient to induce demixing (microphase separation) of the A and B blocks. Indeed, the reduced multiblock Flory parameter $\bar{\chi}_{AB} = N_1\chi_{AB} = 8$ is below the corresponding ODT value for the multiblock AB copolymer[47,48] (here N_1 is the degree of polymerization of one A or B block). The system looks like a symmetric AB-C diblock copolymer and, accordingly, forms a lamellar structure comprised of C- and AB-layers, as is clearly seen in Fig. 5.

Figure 6 shows the color volume density maps for the *parallel* lamellar-*in*-lamellar structure $L_{||}(3)$ of A-(B-*b*-A)$_2$-*b*–C for $\tilde{\chi}_{AB} = 2\tilde{\chi}_{AC} = 100$ and $\tilde{\chi}_{BC} = 40$. Now the AB and C/(AB) incompatibility is stronger and, as a result, two A-layers and one B-layer are formed between two successive C-layers. A further increase of the blocks incompatibility ($\tilde{\chi}_{AB} = 2\tilde{\chi}_{AC} = 120$) (Fig. 7) results in an increase of the number of internal A- (respectively B-) layers up to 3 (respectively 2). In this case the parallel lamellar-*in*-lamellar structure $L_{||}(5)$ appears.

A more quantitative representation of the morphologies visualized in Figs. 6 and 7 as color density maps are provided by the volume fraction profiles presented in Fig. 8. Indeed, it is seen from Figure 8 that, in addition to the strong peaks corresponding to various layers, there are also two weak peaks which describe a weak localization at the A/C interface of some B-blocks, even though they are not directly linked to the C-blocks. The origin of the peaks is illustrated in Fig. 9 for the $L_{||}(3)$ morphology.

Since $\tilde{\chi}_{BC} = 40$ and $\tilde{\chi}_{AB} \geq 100$, the B-blocks are considerably less repulsed by the C-blocks than by the A-ones. So, in the thermodynamic equilibrium the dominant bridge-like chain conformations (like the upper one in Fig. 9) coexist always with a small number of B-loops (light-green) at the A/C interface, which are embedded in the C-domains. Of

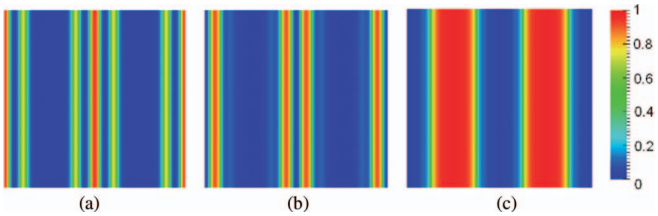

FIG. 7. Volume fraction map for the parallel lamellar-*in*-lamellar structure $L_{||}(5)$ of A-*b*-(B-*b*-A)$_2$-*b*-C with three A-type internal layers at $\tilde{\chi}_{AB} = 2\tilde{\chi}_{AC} = 120$ and $\tilde{\chi}_{BC} = 40$. (a) A blocks; (b) B blocks; (c) C blocks.

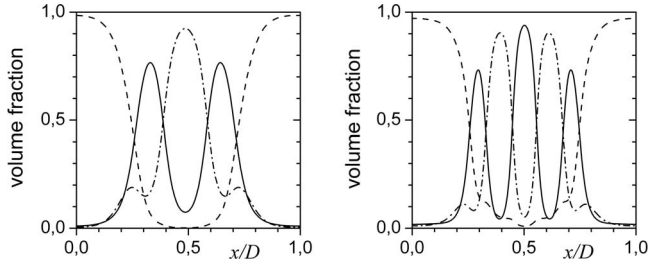

FIG. 8. Composition profiles of A-*b*-(B-*b*-A)$_2$-*b*-C for parallel lamellar-*in*-lamellar. Left: $L_{||}(5)$ at $\tilde{\chi}_{AB} = 2\tilde{\chi}_{AC} = 120$ and $\tilde{\chi}_{BC} = 40$; right: $L_{||}(3)$ at $\tilde{\chi}_{AB} = 2\tilde{\chi}_{AC} = 100$ and $\tilde{\chi}_{BC} = 40$. The solid, dotted–dashed, and dashed lines correspond to the profiles of the A, B, and C components, respectively.

course, it is not very probable that a B-block can reach an A/C interface by passing through the A-barrier. But, as soon as it does, it becomes equally improbable that the B-block will return to the B-layer through the same A-barrier. The actual fraction of B-loops in thermodynamic equilibrium is implicitly calculated within the SCFT as shown in Fig. 8.

B. Perpendicular lamellar-*in*-lamellar morphology

Here the "internal" layers are comprised of A- and B blocks, which are oriented perpendicularly to the C-layers. For the $L_{\perp}$ case (Fig. 10) the composition profiles along the odd and even layers are the same whereas for $SL_{\perp}$ (Fig. 11) the profiles are shifted by half of the period in the vertical direction L_y. It is worth mentioning that the morphologies where the composition profiles along the odd and even layers are shifted by an interval xL_y, $-0.5 < x < 0.5$, were already found for some ternary miktoarm ABC stars.[49] Remarkably, for our linear multiblock ABC copolymers we find that only the morphologies with $x = 0$ and $x = 0.5$ are stable. No intermediate morphologies are observed.

It is also worth noticing that we needed some tricks to reach the stable *perpendicular* lamellar-*in*-lamellar morphologies. The point is that the SCFT numerical procedure outlined in Sec. II is rather sensitive to the initial conditions,[24] which is only natural for the case, when the SCFT equations have many solutions (including those that correspond to metastable states). There is no other remedy against this

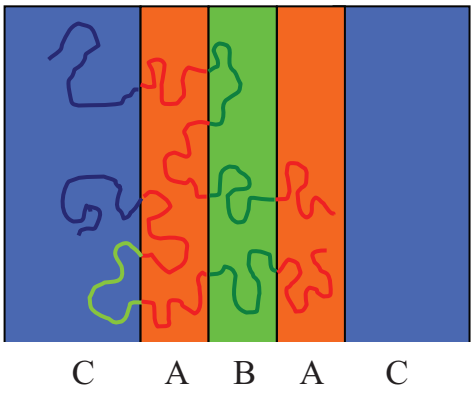

FIG. 9. Schematic illustration of typical conformations contributing to the profiles shown in Figs. 6(a) and 8(b) for $L_{||}(3)$ morphology (see explanation in the text).

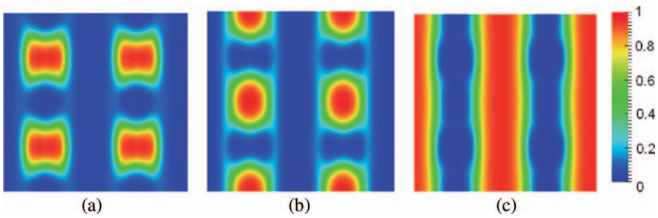

FIG. 10. Volume fraction maps for the metastable *non-shifted perpendicular* lamellar-*in*-lamellar structure $L_\perp$ of A-*b*-(B-*b*-A)$_2$-*b*-C at $\tilde{\chi}_{AB} = 2\tilde{\chi}_{AC} = 120$ and $\tilde{\chi}_{BC} = 20$. (a) A blocks; (b) B blocks; (c) C blocks.

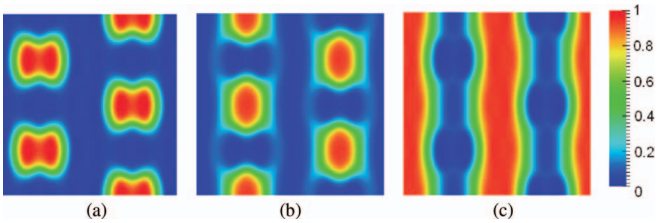

FIG. 11. The volume fraction maps of the stable *shifted perpendicular* lamellar-*in*-lamellar structure $SL_\perp$ of A-*b*-(B-*b*-A)$_2$-*b*-C at $\tilde{\chi}_{AB} = 2\tilde{\chi}_{AC} = 120$ and $\tilde{\chi}_{BC} = 20$. (a) A-blocks; (b) B-blocks; (c) C-blocks.

multiplicity curse but to choose as many physically expected morphologies as possible, to find an initial guess providing convergence to every one of these morphologies and to compare their free energies. So, to find a solution for *perpendicular* lamellar-*in*-lamellar morphologies we have to choose an initial guess possessing the same symmetry. For this purpose we first assume that the A and B components are filling the alternating rectangular domains within the matrix of the C component and next smear the interfaces via proper one-harmonic perturbations of the volume fractions profiles. The subsequent iterations converge to an $L_\perp$ or $SL_\perp$ morphology depending on the initial guess. In fact, we explored all morphologies presented in the phase diagrams shown in Figs. 3 and 4.

Now, let us return to the phase diagrams shown in Figs. 3 and 4. First of all, close to the origin ($\chi_{AB} = 0, \chi_{BC} = 0$), where the interaction between all blocks is weak, the disordered phase is naturally stable. The regions of the DIS phase stability appear topologically equivalent in Figs. 3 and 4 but the disordered phase for A-*b*-(B-*b*-A)$_2$-*b*-C block copolymers is seen to be noticeably more stable than that for the (B-*b*-A)$_2$-*b*-C ones. Next, when the BC incompatibility (i.e., the value of $\tilde{\chi}_{BC}$) is small enough the HEX phase is stable. Both these features are also quite natural. Indeed, the smaller the BC interaction is, the less the ternary block polymer differs from the binary one. When B coincides with C (in terms of the interaction parameters), the (B-*b*-A)$_2$-*b*-C and (A-*b*-(B-*b*-A)$_2$-*b*-C) multiblock copolymers can be considered as asymmetric binary multiblock copolymers $(B_nA_n)_2B_{4n}$ and $(A_nB_n)_2A_nB_{5n}$. The latter consists of more blocks and, therefore,[47,48] is more stable towards microphase separation given the same degree of polymerization. Now, as in most asymmetric AB block copolymers,[50,51] the expected sequence of the order-disorder and order-order transitions is here DIS – body-centered-cubic (BCC) – HEX –LAM, the BCC stability region being usually rather narrow and neglected. This conclusion agrees with the actual transition sequence along the ray *1* in both phase diagrams (see Figs. 3 and 4) for small ratios $\beta = \chi_{BC}/\chi_{AB}$, which is DIS-HEX. The further increase of both the AB and BC blocks incompatibility results in the appearance of the lamellar-*in*-lamellar structures. Therewith, for low temperatures the *parallel* lamellar-*in*-lamellar phases $L_{||}(3)$ and $L_{||}(5)$, respectively, become stable, whereas at intermediate incompatibility (weak and intermediate segregation) the *perpendicular* lamellar-*in*-lamellar structures $L_\perp$ and $SL_\perp$ are stable.

However, the fine structure of these two phase diagrams is rather different. For the (B-*b*-A)$_2$-*b*-C multiblock copolymer (Fig. 3) an increase of the ratio $\beta = \chi_{BC}/\chi_{AB}$ favors stability of the shifted perpendicular phase $SL_\perp$ and the phase transitions sequence with the temperature decrease at low and high values of β (rays *1* and *3* on Fig. 3) are DIS-HEX-$L_\perp$-$L_{||}(3)$ and DIS-$SL_\perp$-$L_{||}(3)$, respectively. Besides, for a restricted interval of intermediate values of β (ray *2* in Fig. 3) the sequence DIS-HEX-$SL_\perp$-$L_\perp$-$L_{||}(3)$ occurs. As far as the A-*b*-(B-*b*-A)$_2$-*b*-C multiblock copolymer (Fig. 4) is concerned, the temperature phase transition sequences are more diverse: DIS-HEX-$L_\perp$-$L_{||}(5)$ (ray *1*), DIS-HEX-$SL_\perp$-$L_\perp$-$L_{||}(5)$ (ray *2*), DIS-HEX-$SL_\perp$-$L_\perp$-$SL_\perp$-$L_\perp$-$L_{||}(5)$ (ray *3*), DIS-HEX-$L_\perp$-$SL_\perp$-$L_\perp$-$L_{||}(5)$ (ray *4*), etc. In other words, a peculiarity of the phase diagram shown in Fig. 4 is the presence of re-entrant (with temperature) $SL_\perp$-$L_\perp$ transitions.

Being discovered via straightforward numerical calculations, these re-entrant transitions hardly have a simple physical explanation. Nevertheless, we dare to see their counterpart in re-entrant (with architecture) conformation behavior we found earlier[25] in multiblock copolymers and suggest that they are the results of a subtle interplay of entropic (due to conformation distortion) and energetic effects under weak and intermediate segregation of A-*b*-(B-*b*-A)$_2$-*b*-C block copolymers.

Next we proceed to get more insight in the $L_\perp$ and $SL_\perp$ morphologies for the A-*b*-(B-*b*-A)$_2$-*b*-C multiblock copolymer. For the particular set of interaction parameters values selected in Figures 9 and 10, the shifted $SL_\perp$ structure is stable and the non-shifted $L_\perp$ is metastable (compare with the phase diagram in Fig. 4).

Similar volume fraction profile maps can be presented for the (B-*b*-A)$_2$-*b*-C multiblock copolymer (not shown).

To obtain some insight into the physical reasons of the *perpendicular* lamellar-*in*-lamellar phases formation we consider the folding of the copolymer chains under study in the two structures $L_\perp$ and $SL_\perp$ in more detail. To this end we present the volume fraction maps for the most relevant parts of the chains. Fig. 12(a) shows the volume fraction map of the A blocks of (B-*b*-A)$_2$-*b*-C that are directly connected to the long C blocks under conditions where $L_\perp$ is the equilibrium state. Because of this connection these A blocks are near the AC interface. The A blocks that are not directly linked to the C blocks form the core of the structure (Fig. 12(b)). The first B blocks that are connected at both ends to A blocks are preferentially present near the AB interface but also near the AC interface where they shield the AC interactions (Fig. 12(c)). The B end blocks form the core of the B domains but are also present at the AC interface (Fig. 12(d)).

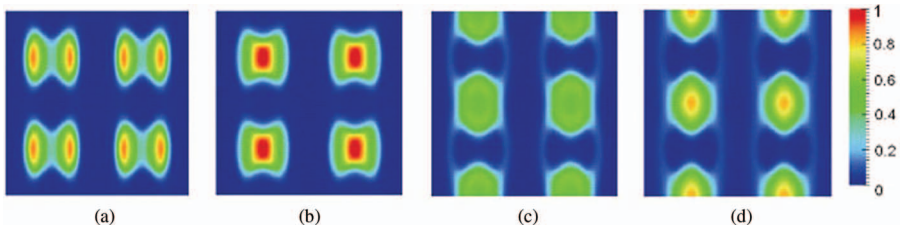

FIG. 12. Volume fraction maps of the different A and B blocks of the multiblock part of the (B-*b*-A)$_2$-*b*-C multiblock copolymers at $\tilde{\chi}_{AB} = 2\tilde{\chi}_{AC} = 120$ and $\tilde{\chi}_{BC} = 12$ where $L_\perp$ is the equilibrium state. (a) A blocks connected to the C blocks; (b) the rest of A blocks; (c) the B blocks that are connected at both ends to an A block; (d) the end B blocks.

Another interesting observation is that the AC interface is not a straight line for the *perpendicular* lamellar-*in*-lamellar structures, as would be required to minimize the number of unfavorable contacts between the A and C monomers (Figs. 10 and 11). This is due to the fact that the interface is formed by the junction points between the A and C blocks. As we discussed earlier,[21] the C blocks have to fill a space equal to the volume of the A and B blocks together. As a consequence, the C blocks are stretched in the direction perpendicular and parallel to this interface. In order to fill this space uniformly, and in particularly the region opposite the B phase, the polymers should be stretched a lot at the AC interface and much less far away from the interface. To minimize the stretching close to the interface the shape of the interface becomes curved inwards into the region of the C blocks. The distance between successive AC junction points increases and the stretching energy of the C blocks decreases. Additionally the B blocks that are also present at the AC interface reduce the interfacial energy.

As shown in Figs. 10(c) and 11(c), the shape of the interface between the C-blocks and AB-blocks looks sinusoidal. In Fig. 10(c), corresponding to the $L_\perp$ structure, the AC interfaces in successive layers are in phase, whereas in Fig. 11(c), corresponding to $SL_\perp$ phase, they are shifted by a half-period. Obviously this difference affects also the stretching of the long C blocks.

To illustrate this, the volume fraction maps of the ends of the C blocks are presented in Figure 13. For the non-shifted $L_\perp$ (Fig. 13(a)) the concentration of the open ends exhibits maxima. Not surprisingly, they are located in the middle of the C layers opposite the middle of the domains formed by the B blocks. In the shifted $SL_\perp$ case the C ends are distributed more uniformly along the midplane of the C layers with less pronounced maxima in front of the AB interfaces. In other words, the entropic loss for the shifted perpendicular morphology is less than that for the non-shifted one. This might be one of the reasons why the shifted structure is usually the preferred state when the energetic gain is not too big, i.e., in the region where $\tilde{\chi}_{AB} = 2\tilde{\chi}_{AC}$ is not too large.

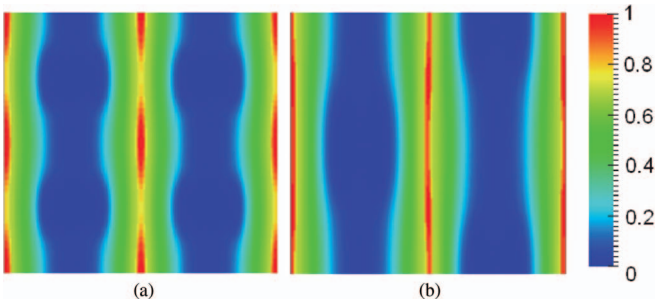

FIG. 13. Volume fraction maps of the free ends of C blocks of (B-*b*-A)$_2$-*b*-C for $\tilde{\chi}_{AB} = 2\tilde{\chi}_{AC} = 120$ and $\tilde{\chi}_{BC} = 17$. (a) Non-shifted structure $L_\perp$ (equilibrium state); (b) shifted structure $SL_\perp$.

It is worth noticing that the periods along the AB and AC interfaces (L_x and L_y, respectively) are, in general, different for the $SL_\perp$ and $L_\perp$ structures. In the stability region of $L_\perp$ for the (B-b-A)$_2$-b-C architecture L_y is slightly bigger and L_x less for the $L_\perp$ structure than for the metastable $SL_\perp$ structure. On the transition line between $L_\perp$ and $SL_\perp$ L_x and L_y are equal for both morphologies. When the $SL_\perp$ structure is stable it becomes more extended in the y direction than for the metastable $L_\perp$.

IV. CONCLUSION

Summarizing, we used the SCFT numerical procedure to study the order-disorder and order-order phase transitions between the planar ordered phases in two types of multiblocks copolymers, (B-b-A)$_2$-b-C and A-b-(B-b-A)$_2$-b-C for typical values of the component volume fractions $\varphi_C = 0.5$, $\varphi_A = \varphi_B = 0.25$ and the ratio of the interaction parameters $\tilde{\chi}_{AB}/\tilde{\chi}_{AC} = 2$. The hexagonal, *parallel* lamellar-*in*-lamellar (LIL) $L_{||}(n)$ (including the simple lamellar $L_{||}(1)$) as well as *non-shifted* and *shifted* ($L_\perp$ and $SL_\perp$) perpendicular LIL morphologies are found to be stable depending on the values of the reduced interaction parameters $\tilde{\chi}_{AB}$, $\tilde{\chi}_{BC}$ and the corresponding phase diagrams are presented. The *perpendicular* LIL are found to occur in the realm of weak and intermediate segregation whereas the *parallel* ones belong to that of stronger segregation. For a specific choice of the chemical nature of the repeated units A, B, and C the temperature evolution of the ordered morphologies depends on the value of the ratio $r = \Theta_{AB}/\Theta_{BC}$, where Θ is the corresponding characteristic temperature. For the (B-b-A)$_2$-b-C multiblock copolymers, the sequence of successive phases as the temperature decreases reads DIS – HEX – $L_\perp$ – $L_{||}(3)$ at bigger r, whereas for smaller r it is DIS – HEX – $SL_\perp$ – $L_{||}(3)$, in a comparatively narrow intermediate interval of r the phase transition sequence DIS – HEX – $SL_\perp$ – $L_\perp$ – $L_{||}(3)$ holds. Due to the extra A-block and the concurrent difference in A- and B-block lengths, the phase diagram of the A-b-(B-b-A)$_2$-b-C multiblock copolymer turned out to be more complex than that of (B-b-A)$_2$-b-C. Here the sequence of the phase transitions also

depends on r, but the re-entrant (with temperature) phase transitions $SL_\perp - L_\perp$ are rather rule than an exception. Calculating and analyzing the volume fraction profiles of the free ends of the C-blocks shows that these phase transitions are accompanied by a redistribution of the free C-ends along the mid-plane as well as a change of the geometric parameters of the lattice cell. An interesting option to be studied elsewhere is that the re-entrant phase transitions found are related to an effect of incommensurability between the cell periods and the end blocks gyration radii.

There is one more interesting issue, which deserves a special remark. Since all lamellar (including lamellar-*in*-lamellar) morphologies are, effectively, 1D systems, it could seem that it makes not much sense to build the phase diagrams containing two and more regions of such 1D morphologies. Indeed, due to the famous Landau theorem,[52] the actual structure observed throughout the sample under consideration would be a random mixture of slices corresponding to various lamellar morphologies even though the most favorable one can be distinguished. However, the observable (average) volume fraction of the slices corresponding to the most favorable lamellar morphology is expected to be close to unity since the characteristic width D of these slices is rather big ($D \sim \exp(2E/T)$, where E is the surface energy per the total area of a junction between various morphologies). Thus, the phase diagram we built here is a rather good approximation to the reality.

We believe that the results obtained are applicable, *mutatis mutandis,* to other multiblock ternary ABC copolymers.

[1] J. Ruokolainen, R. Mäkinen, M. Torkkeli, T. Mäkelä, R. Serimaa, G. ten Brinke, and O. Ikkala, Science **280**, 557 (1998).
[2] J. Ruokolainen, G. ten Brinke, and O. Ikkala, Adv. Mater. **11**, 777 (1999).
[3] O. Ikkala and G. ten Brinke, Science **295**, 2407 (2002).
[4] J. Masuda, A. Takano, J. Suzuki, Y. Nagata, A. Noro, K. Hayashida, and Y. Matsushita, Macromolecules **40**, 4023 (2007).
[5] J. Masuda, A. Takano, Y. Nagata, A. Noro, and Y. Matsushita, Phys. Rev. Lett. **97**, 098301 (2006).
[6] M. G. Faber, V. S. D. Voet, G. ten Brinke, and K. U. Loos, Soft Matter **8**, 4479 (2012).
[7] G. Fleury and F. S. Bates, Macromolecules **42**, 1691 (2009).
[8] G. Fleury and F. S. Bates, Macromolecules **42**, 3598 (2009).
[9] A. F. Thünemann and S. General, Macromolecules **34**, 6978 (2001).
[10] C. Osuji, C. Y. Chao, I. Bita, C. K. Ober, and E. L. Thomas, Adv. Funct. Mater. **12**, 753 (2002).
[11] I. A. Ansari, V. Castelletto, T. Mykhaylyk, I. W. Hamley, Z. B. Lu, T. Itoh, and C. T. Imrie, Macromolecules **36**, 8898 (2003).
[12] B. Nandan, C. H. Lee, H. L. Chen, and W. C. Chen, Macromolecules **38**, 10117 (2005).
[13] I. W. Hamley, V. Castelletto, P. Parras, Z. B. Lu, C. T. Imrie, and T. Itoh, Soft Matter **1**, 355 (2005).
[14] R. Nap, C. Kok, G. ten Brinke, and S. I. Kuchanov, Eur. Phys. J. E **4**, 515 (2001).
[15] Y. Smirnova, G. ten Brinke, and I. Ya. Erukhimovich, Polym. Sci., Ser. A **47**, 430 (2005).
[16] Y. Smirnova, G. ten Brinke, and I. Ya. Erukhimovich, J. Chem. Phys. **124**, 054907 (2006).
[17] S. I. Kuchanov, V. E. Pichugin, and G. ten Brinke, Europhys. Lett. **76**, 959 (2006).
[18] A. Subbotin, T. Klymko, and G. ten Brinke, Macromolecules **40**, 2915 (2007).
[19] T. Klymko, A. Subbotin, and G. ten Brinke, J. Chem. Phys. **129**, 114902 (2008).
[20] T. Klymko, V. Markov, A. Subbotin, and G. ten Brinke, Soft Matter **5**, 98 (2009).
[21] A. Subbotin, V. Markov, and G. ten Brinke, J. Phys. Chem. B **114**, 5250 (2010).
[22] R. Nap, I. Ya. Erukhimovich, and G. ten Brinke, Macromolecules **37**, 4296 (2004).
[23] R. Nap, N. Sushko, I. Ya. Erukhimovich, and G. ten Brinke, Macromolecules **39**, 6765 (2006).
[24] Y. A. Kriksin, I. Ya. Erukhimovich, P. G. Khalatur, Y. Smirnova, and G. ten Brinke, J. Chem. Phys. **128**, 244903 (2008).
[25] Y. A. Kriksin, I. Ya. Erukhimovich, Y. Smirnova, P. G. Khalatur, and G. ten Brinke, J. Chem. Phys. **130**, 204901 (2009).
[26] W. Li and A.-C. Shi, Macromolecules **42**, 811 (2009).
[27] Y. Xu, W. Li, F. Qiu, Y. Yang, and A.-C. Shi, Phys. Chem. Chem. Phys. **13**, 12421 (2011).
[28] L. Wang, J. Lin, and L. Zhang, Macromolecules **43**, 1602 (2010).
[29] Y. Xu, W. Li, F. Qiu, Y. Yang, and A.-C. Shi, J. Phys. Chem. B **114**, 14875 (2010).
[30] M. W. Matsen and M. Schick, Phys. Rev. Lett. **72**, 2660 (1994).
[31] F. Drolet and G. H. Fredrickson, Phys. Rev. Lett. **83**, 4317 (1999).
[32] J. G. E. M. Fraaije, J. Chem. Phys. **99**, 9202 (1993).
[33] N. M. Maurits and J. G. E. M. Fraaije, J. Chem. Phys. **107**, 5879 (1997).
[34] E. Helfand and Z. R. Wasserman, in *Developments in Block Copolymers*, edited by I. Goodman (Applied Science, London, 1982), p. 99.
[35] E. Helfand and Z. R. Wasserman, Macromolecules **9**, 879 (1976).
[36] M. W. Matsen, Phys. Rev. Lett. **74**, 4225 (1995).
[37] M. D. Feit, J. A. Fleck, and A. Steiger, J. Comput. Phys. **47**, 412 (1982).
[38] K. O. Rasmussen and G. Kalosakas, J. Polym. Sci., Part B: Polym. Phys. **40**, 1777 (2002).
[39] H. D. Ceniceros and G. H. Fredrickson, Multiscale Model. Simul. **2**, 452 (2004).
[40] G. H. Fredrickson, *The Equilibrium Theory of Inhomogeneous Polymers* (Oxford University Press, New York, 2006).
[41] K.-C. Ng, J. Chem. Phys. **61**, 2680 (1974).
[42] R. B. Thompson, K. Ø. Rasmussen, and T. Lookman, J. Chem. Phys. **120**, 31 (2004).
[43] P. Stasiak and M. W. Matsen, Eur. Phys. J. E **34**, 110 (2011).
[44] J.-L. Barrat, G. H. Fredrickson, and S. W. Sides, J. Phys. Chem. B **109**, 6694 (2005).
[45] Y. A. Kriksin and P. G. Khalatur, Macromol. Theory Simul. **21**, 382 (2012).
[46] C. A. Tyler and D. C. Morse, Macromolecules **36**, 8184 (2003).
[47] I. Ya. Yerukhimovich, Polym. Sci. USSR **24**(9), 2232 (1982).
[48] H. Benoit and G. Hadziioannou, Macromolecules **21**, 1449 (1988).
[49] Y. Xu, W. Li, F. Qiu, H. Zhang, Y. Yang, and A.-C. Shi, J. Polym. Sci., Part B: Polym. Phys. **48**, 1101 (2010).
[50] L. Leibler, Macromolecules **13**, 1602 (1980).
[51] I. Erukhimovich, Eur. Phys. J. E **18**, 383 (2005).
[52] L. D. Landau and E. M. Lifshitz, *Statistical Physics, Part 1*, 3rd ed. (Pergamon Press, Oxford, 1980).